Comparing Landslide Mapping from DTM Satellite Derived Data and Field Based Studies of Loess Sediments in Western China

Philip Leopold, Wang Tao, Roland Perko, Gerhard Heiss, Martin Jung, Armin Oblin, and Yongshuang Zhang

Abstract

This paper focuses on experiences gained by creating a landslide inventory map for a study area of approx. 850 km^2 near the city of Tianshui in Gansu province, Western China. The study area consists of a Loess landscape that is strongly anthropogenic transformed by terraced agriculture and is interspersed by mainly earthquake triggered landslides. Two different approaches were performed to establish an inventory map of landslides: Mapping landslides from field based studies and mapping landslides from a DTM derived from a Pléiades satellite image pair. Pléiades images offer a panchromatic ground sampling distance of 0.5 m which enabled us to create a Digital Terrain Model (DTM) with a resolution of 1.0 m. The methodologies of these two landslide mapping approaches are presented and respective results are compared showing advantages and disadvantages of each approach. One of the main results of the project was to demonstrate the applicability and the effectiveness of DTM mapping in Loess sediments of Western China. In comparison to field mapping, the DTM inventory is at least of equal quality as the field mapped inventory because of its consistency and completeness. DTM mapping is also a much more cost efficient tool, especially when looking at mapping larger areas in remote locations in Western China, as well as those areas which are difficult to access.

Keywords

Landslide mapping • Loess • Western China • Digital elevation model • Pléiades • Landslide inventory • Earthquake induced landslides

P. Leopold (✉) · G. Heiss · M. Jung · A. Oblin
Energy Department, AIT Austrian Institute of Technology GmbH, Donau-City-Straße 1, 1220 Vienna, Austria
e-mail: philip.leopold@ait.ac.at

G. Heiss
e-mail: gerhard.heiss@ait.ac.at

M. Jung
e-mail: martin.jung@ait.ac.at

A. Oblin
e-mail: armin.oblin@gmx.at

W. Tao · Y. Zhang
Chinese Academy of Geological Sciences, Institute of Geomechanics, No. 11 Minzudaxue Nanlu, Haidian District, Beijing, 100081, People's Republic of China
e-mail: wangtao_ig@163.com

Y. Zhang
e-mail: zhys100@hotmail.com

R. Perko
Joanneum Research Digital, Steyrergasse 17, 8010 Graz, Austria
e-mail: roland.perko@joanneum.at

M. Mikoš et al. (eds.), *Advancing Culture of Living with Landslides*,
DOI 10.1007/978-3-319-53498-5_11

Introduction

In course of an ongoing Chinese-Austrian scientific cooperation project landslide susceptibility modeling was applied for a study area near the city of Tianshui in Gansu province, China. The study area consists of a Loess landscape that is strongly anthropogenic transformed by terraced agriculture and is interspersed by mainly earthquake triggered landslides.

This paper focuses on our experiences gained by creating a landslide inventory map for this region, which was later used as input parameter for landslide susceptibility modeling. Two different approaches were performed to establish the landslide inventory map: Mapping landslides from field based studies and mapping landslides from a DTM derived from a Pléiades satellite image pair. We will compare these approaches and show advantages and disadvantages of each approach.

Characteristics of the Study Area

The study area (Fig. 1) shows a geomorphological position at the northeastern margin of the Tibetan Plateau, it also belongs to the southern edge of Long-Zhong loess hilly area. Sandu River and its tributary Qingxi River basins cover most of the area, in the southern border area the Weihe River Valley can be found. The regional annual average rainfall is about 500 mm, and evaporation is about 2.5 times to precipitation, so the climate is relatively dry (Cheng et al. 2007).

Referring to the geological structure and earthquake context, the study area is located in the aggregation part of Qinghai Tibet plate, North China plate and the Yangtze plate (Zhang and Xie 1991). The regional geological structure is very complex. The main active structures related to landslide occurrence in the area include the northern margin of west Qinling fault zone located in southwest part and the buried Tongwei fault located in northeast part (Shao et al. 2011; Zhou et al. 1991). The study area is located in the eastern section of the Tianshui-Lanzhou seismic zone, the seismic background is complex with frequent seismic activities. The main seismogenic tectonic west Qinling fault zone caused two earthquakes with a magnitude of 7.0–7.9 and three 6.0–6.9 earthquakes in the past three centuries. Weak earthquakes also occurred as belts and also crustal deformation measurement data confirmed the current fault activity (Kang et al. 1999; Shao et al. 2011).

The geological setup consists mainly of Cretaceous conglomerates and Neogene mudstones and silty mudstones forming the bedrock. These sediments are covered by Pleistocene Loess deposits of different age, reaching a total thickness from a view meters up to several 10 m (Pei et al. 2004).

Landslides in the study area can be mainly divided into two types:

(1) Deep-seated mudstone landslides induced by historical strong earthquakes. Most of these landslides were induced by Tongwei M7.5 earthquake in 1718 (Chen and Shi 2006; Gu 1983). The sliding surfaces are mostly deep seated in Neogene mudstones. The sliding mass depth is generally up to tens of meters or more, so the landslides usually have a large volume. Referring to the geometrical characteristics, although the landslide scarps are mostly clear, the lateral boundaries of contiguous landslides are usually intertwined and are therefore difficult to distinguish. Because of this, many landslides often form into landslide clusters. These landslides also have huge disaster effects.
(2) Shallow landslides mostly induced by heavy rainfall. These kinds of landslides may consist of two types: (A) Sliding mass and slide plane are within the pure loess layer; (B) Sliding mass mainly consists of loess and the slide plane is located at the interface between loess and Neogene mudstone. All of these landslides are mainly controlled by vertical joints and rainfall infiltration. Compared to the large-scale seismic landslides, they occur more frequently and numerous and the disaster effect is relatively small.

Methodology

General Approach

Within the above mentioned project, field based studies were carried out in the second half of 2014 by a Chinese expert team. Based on these findings, an Austrian expert team performed a landslide susceptibility modeling in the first half of 2015. As a high resolution DTM was needed to perform this modelling, we came up with the idea to also perform a "second" landslide mapping solely based on the high resolution DTM in order to compare the two mapping results (which is the topic of this paper). So the team that performed the field mapping did not know the results of the DTM mapping, but the DTM mapper did know the results of the field mapping. However, the DTM based mapping of landslides was performed without taking any field mapping results into account. The DTM mapping was performed as indenpendent task, from an Austrian expert who had no field experience in China.

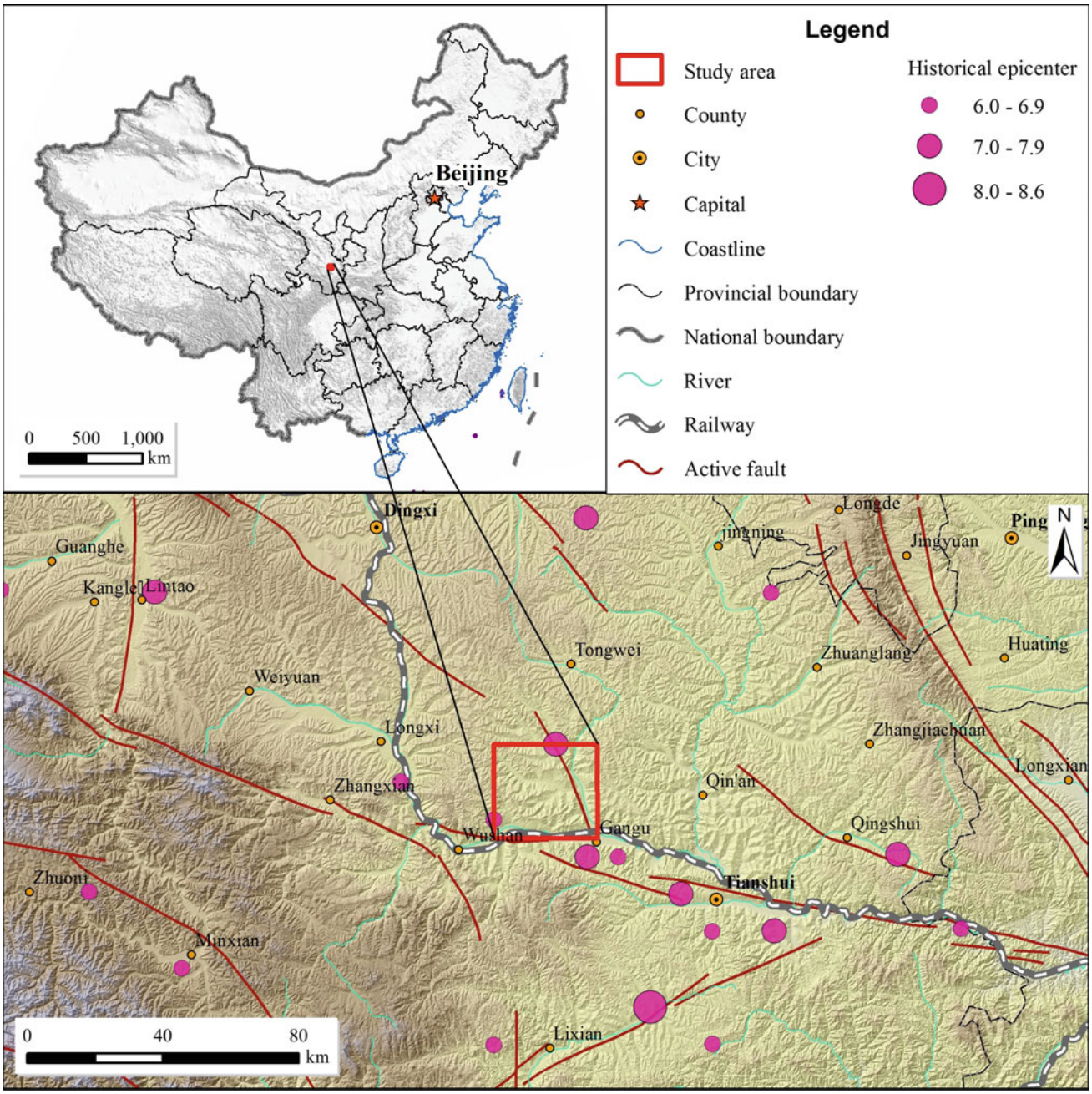

Fig. 1 Geographical location map of the study area near the city of Tian Shui

Field Based Studies

Field based studies were performed by field investigation and supported from remote sensing images and a DTM derived from Chinese resource satellite ZY-3. The spatial resolution of ZY-3 optical images are 2.5 m. The spatial resolution of the DTM derived from ZY-3 data is 10.0 m. The specific study processes consists mainly of 4 steps:

(1) For a basic field work map, the ZY-3 optical images are georeferenced and plotted using GIS software;
(2) In the field, potential landslides are sketched on this field map and basic characteristics of landslides are recorded. Because of the scant vegetation young and even old landslides are very good visible;
(3) Mapped landslides are sketched as polygons using GIS software;

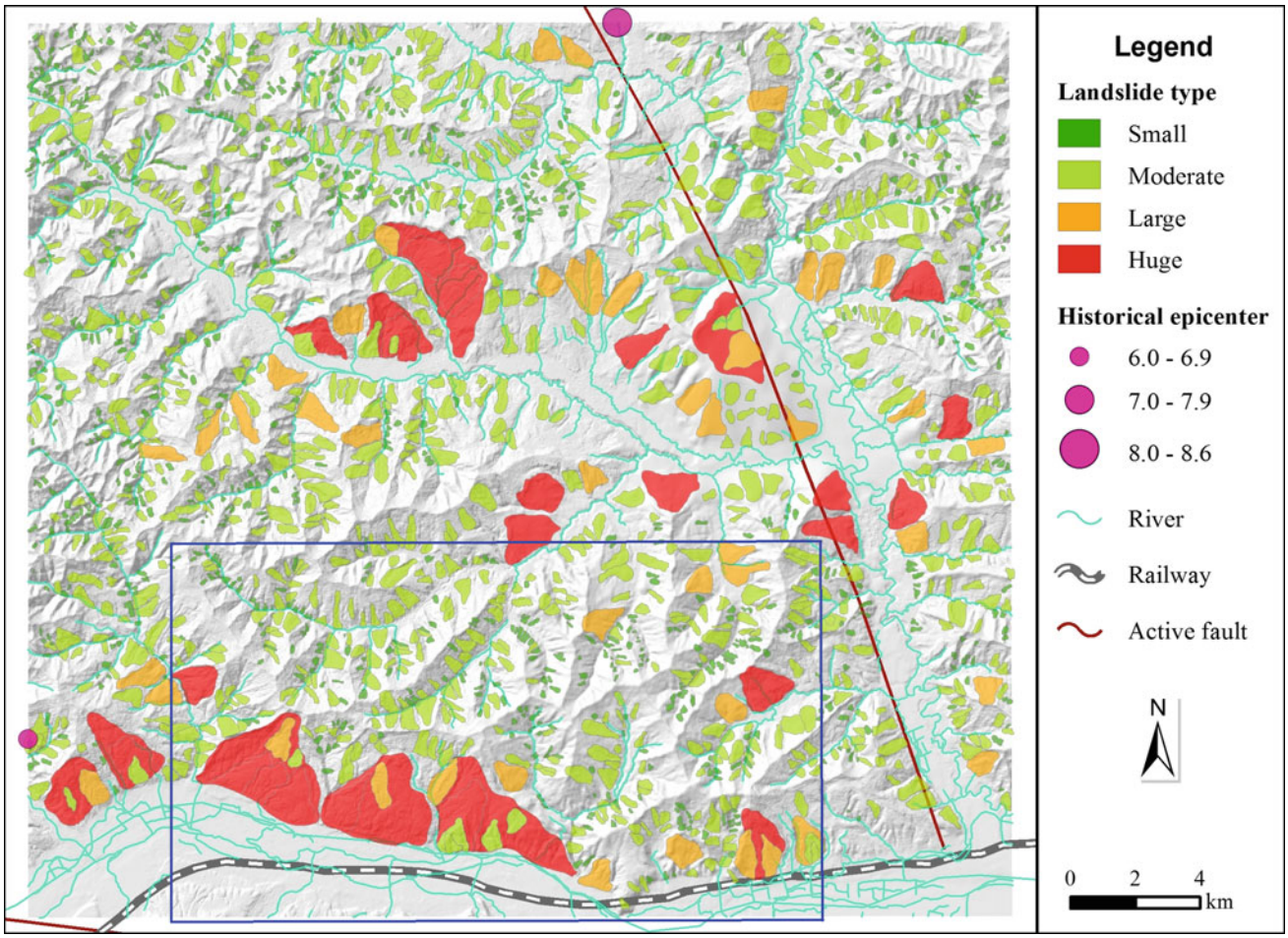

Fig. 2 Landslide inventory map based on field mapping. The *blue rectangle* shows the area that also has been mapped DTM based

(4) Based on the calculated landslide polygon area landslides are classified into 4 types: huge, large, moderate, small.

Following this process, a landslide inventory map of the study area is produced (Fig. 2). We totally mapped 1897 landslide polygons which cover 227.13 km^2 out of the study area of 845.23 km^2. Huge landslides (the moved mass from each landslide has an extention of more than 1 km^2) cover a total area of 50.29 km^2, large landslides (0.5–1 km^2) cover 30.42 km^2, the moderate (0.05–0.5 km^2) cover 121.41 km^2 and small landslides (smaller than 0.05 km^2) cover 25.01 km^2.

According to the geometric characteristics of earthquake induced loess landslides in western China and our own inventory result (Chen and Shi 2006; Lu et al. 2006; Wang and Wang 2013), we deduce that the vast majority of huge and most large landslides are probably induced by historical mega earthquakes. An example is the precise record of a huge landslide triggered by Tongwei M7.5 earthquake in 1718 in Yongning town (Chen and Shi 2006). The macroscopic epicenter of Tongwei earthquake was just located in the north margin of the study area (Fig. 1). The epicenter is only about 14 km far from the geometric center of study area.

We also believe that most of the small and moderate landslides are more likely induced by precipitation.

Creating a Local DTM from a Pléiades Satellite Image Pair

A high resolution DTM (e.g. resulting from airborne laser-scanning) was not available for the study area for landslide mapping, as such models are commonly not available in China. Within the given time frame and ressources a suitable model could only be achieved by using satellite data. After extensive research a pair of Pléiades satelitte images was acquired, covering a total area of 395 km^2 and an essential part (236 km^2) of the study area (Fig. 2). The image pair is suitable to create a DTM with a resolution of 1.0 m of the area. The Pleaides images were delivered with a ground

Table 1 Acquisition parameters of the Pléiades stereo data taken on 2014-05-07 with a base-to-height ratio of 0.403 and an intersection angle of 22.8°

Time	Incidence angles (°)		
	Across	Along	Overall
3:53:38.3	0.75	−10.54	10.56
3:54:15.4	−4.54	11.68	12.48

sampling distance of 0.5 m (panchromatic) and 2.0 m (multi-spectral), where only the panchromatic information was used for stereo processing. For detailed acquisition parameters see Table 1.

For this project the Pléiades initial 2D and 3D geo-location accuracy was considered to be high enough, such that the stereo-processing was applied without parameter adjustment of the initial sensor models. For the generation of the digital surface model (DSM) from the given stereo pair, the following procedures were applied (similar to (Perko et al. 2014)):

- *Epipolar rectification* of both stereo images based on the initial sensor models, such that a pre-defined point in the reference image can be found along a horizontal line in the search image. While the concept of epipolar geometry was first realized for perspective images, appropriate implementations were further made for Pléiades-like pushbroom geometries (Wang et al. 2011) and for SAR geometries (Gutjahr et al. 2014). In either case the generation of epipolar image pairs is based on the underlying sensor geometries and relies on accurate sensor models in order to achieve pairs with strictly corresponding image lines.
- *Image matching* in order to find correspondences of reference image pixels in the search image. In case of epipolar images highly sophisticated image matching algorithms can be applied which utilize the fact that the search is restricted to one dimension and thus local and also global optimization methods can achieve highly accurate results at fast runtimes. A good overview and benchmark of such algorithms is given in (Scharstein and Szeliski 2002). For this work a custom-tailored version of the semi-global matching (SGM) algorithm, which was introduced by Hirschmüller (2008), was used. Disparity predictions can be calculated based on the sensor models and coarse elevation data (e.g. the SRTM DSM), such that the search range of the SGM algorithm can be limited. The cost function compares two image patches and is defined as the Hamming distance of the two Census transforms within 9 × 9 pixel windows on the epipolar images. Within the semi-global optimization an adaptive penalty is used to preserve 3D breaklines. The image matching procedure yields two dense disparity maps pointing from the reference to the search image and vice versa.
- *Spatial point intersection*, in order to calculate the ground coordinates from the corresponding image pixels retrieved from image matching by means of a least squares approach. To some extent, unreliable matching results can be identified and rejected in this step. This procedure results in a "cloud" of 3D points, irregularly distributed on ground.
- *DSM resampling*, i.e. interpolation of a regular raster of height values from these 3D points. Remaining gaps may be filled using an appropriate interpolation mechanism.
- *DSM fusion* to combine the information of forward and backward matching. Here the method described in Rumpler et al. (2013) is applied, which takes all height measurements within a 3 × 3 neighborhood and extracts the mode of this height distribution. Thus, local height errors can rather be eliminated than by a straightforward median based approach.

Figure 3 visualizes the ortho image of the region together with the extracted DSM (shaded relief) with 1 m spacing together with a small subset of 3.4 km^2 where the terraced agriculture is very well visible in the 3D model (actually the mentioned matching extension that preserves 3D breaklines helps in correctly reconstructing such terrain features). The ortho images are based on pansharpened images, which are just used for visualization in this study. Obviously, the presented stereo processing workflow produces a DSM where also man-made structures like buildings and vegetation are visible. However, due to low vegetation height in the critical landslide regions, there the DSM can be considered as a DTM.

DTM Based Landslide Mapping

As explained above, for the present work a DTM with a resolution of 1 m from a Pléiades 50 cm PAN stereo pair was created. It covers a 236 km^2 portion in the south of our above-mentioned study area. In comparison to other digital terrain data with 20 m or 10 m resolution, this model offers the best foundation for mapping landslides in our study area. Not only smaller structures, such as small stream channels and gullies, can be detected, but also contours and break lines are much sharper depicted, as shown in Fig. 4.

In general, digital terrain models also allow a variety of computerized morphometric and morphologic analysis.

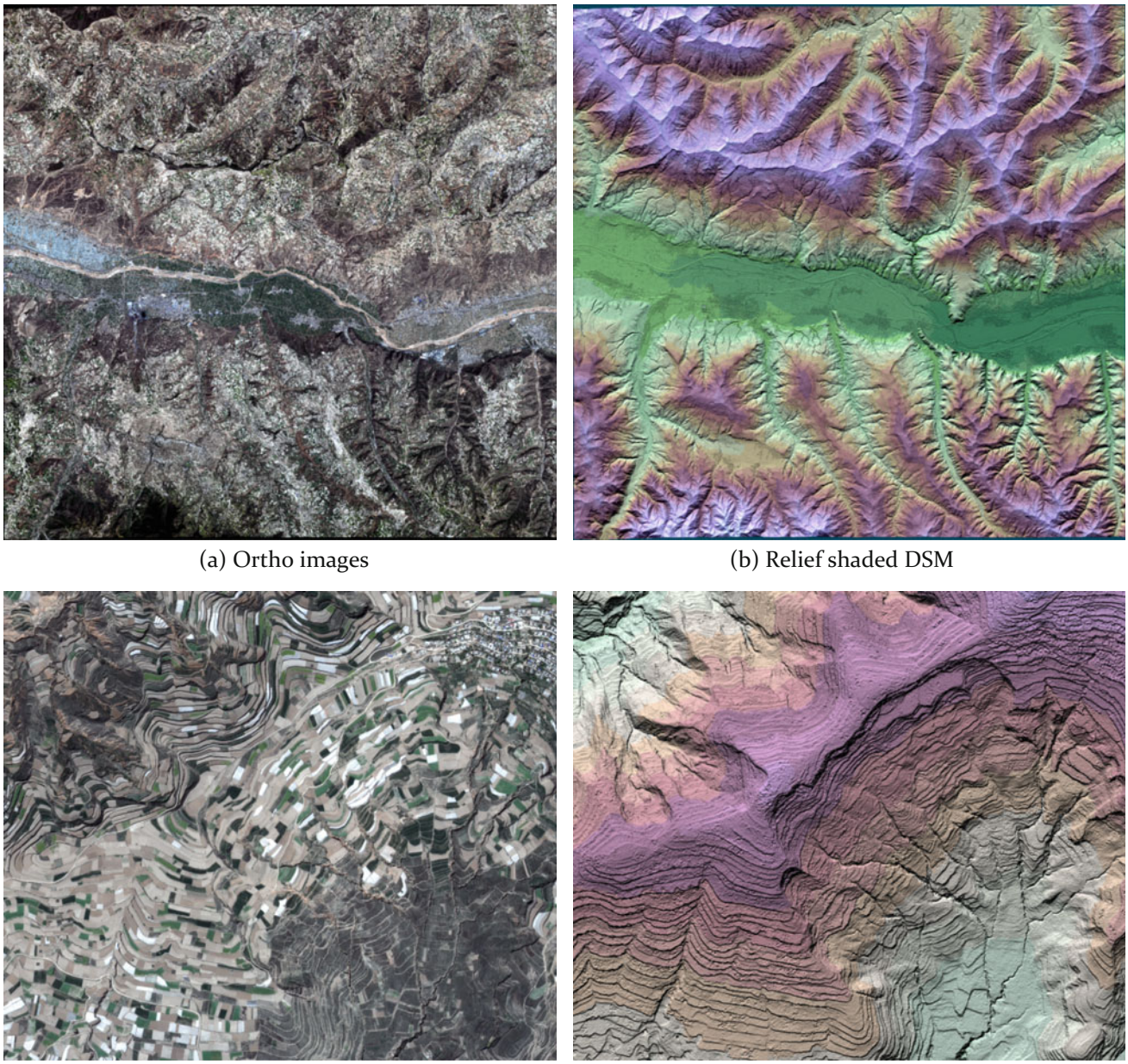

(a) Ortho images (b) Relief shaded DSM

(c) Detailed view on ortho image (d) Detailed view on relief shaded DSM

Fig. 3 (**a**, **b**) Ortho image and shaded relief DSM covering 394.4 km^2 and a height range of 1200–2100 m; (**c**, **d**) detailed view of a smaller area with 2001 × 1701 m^2 (3.4 km^2) and a height range of 1380–1780 m. The ortho images where pansharpened just for visualization

Numerous attempts have been undertaken for automated classification of topography and geomorphology (e.g. Jie Dou et al. 2015; or Kalbermatten et al. 2012), but most articles are dealing with hydrologic effects on the surface. Certainly it is a great challenge for image recognition or pattern perception techniques to digitally automatize landslide mapping. However, in our current approach we chose a knowledge-based approach with manual mapping by visual interpretation which can be performed with any common GIS software.

Simply using the slope representation of the DTM dataset, landslide polygons were manually delineated after a short time of visual learning (as mentioned above, the mapping expert had no field experience in China). From the position of the landslides to each other and their size and relief statements about their relative ages can be made. Also

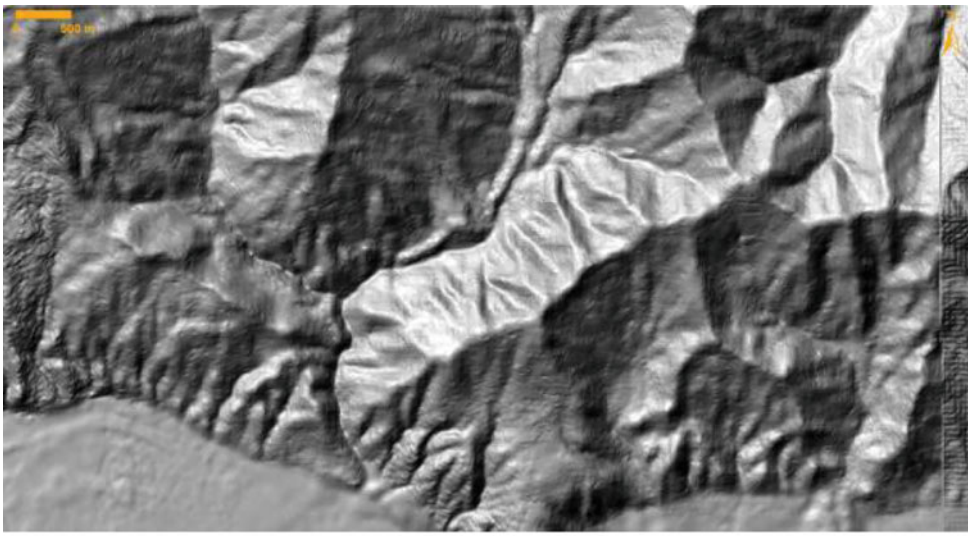

Fig. 4 Comparison of a DTM with 10 m resolution and 1 m resolution in the study area. Only the 1 m model enables a reliable detection of landslides and their precise borders. Compare to Fig. 5 for scale

in many cases, the edge characteristics (steepness, extension) of the mapped landslides give a good hint, whether it is a deep seated or shallow slide.

In total, 562 landslide polygons and 1173 landslide scarp points were mapped in an area of 236 km^2 based on the DTM.

Comparison of Mapping Results

To compare mapping results from field based studies and from DTM derived data we are taking only the results of the above mentioned sub area of 236 km^2 into account (Figs. 2 and 5). For this area, the field based inventory includes 573 landslides; the DTM inventory counts 11 landslides less. However, the location and the coverage of the landslides differ between the two inventories. The DTM inventory overlaps only with 68% of the field-mapped inventory concerning location, but DTM inventory covers 25% more area in total. As visible in Fig. 5, there are certain locations where landslides were mapped in the field but not in the digital model. On the other hand the borders of most large landslides were mapped more wide-stretched and probably more precisely by using the DTM.

We think that these differences are mainly based on the often restricted visibility and limited accessibility when performing ground based fieldwork. The consistent image quality and the bird's eye view of the DTM supports an overall constant quality of the morphological assessment. This makes it easier to differentiate between landslides and slopes without landslides. Furthermore more exact delineations of landslides are possible. Some differences could also be explained with varying spatial references in the base data for the field mapping.

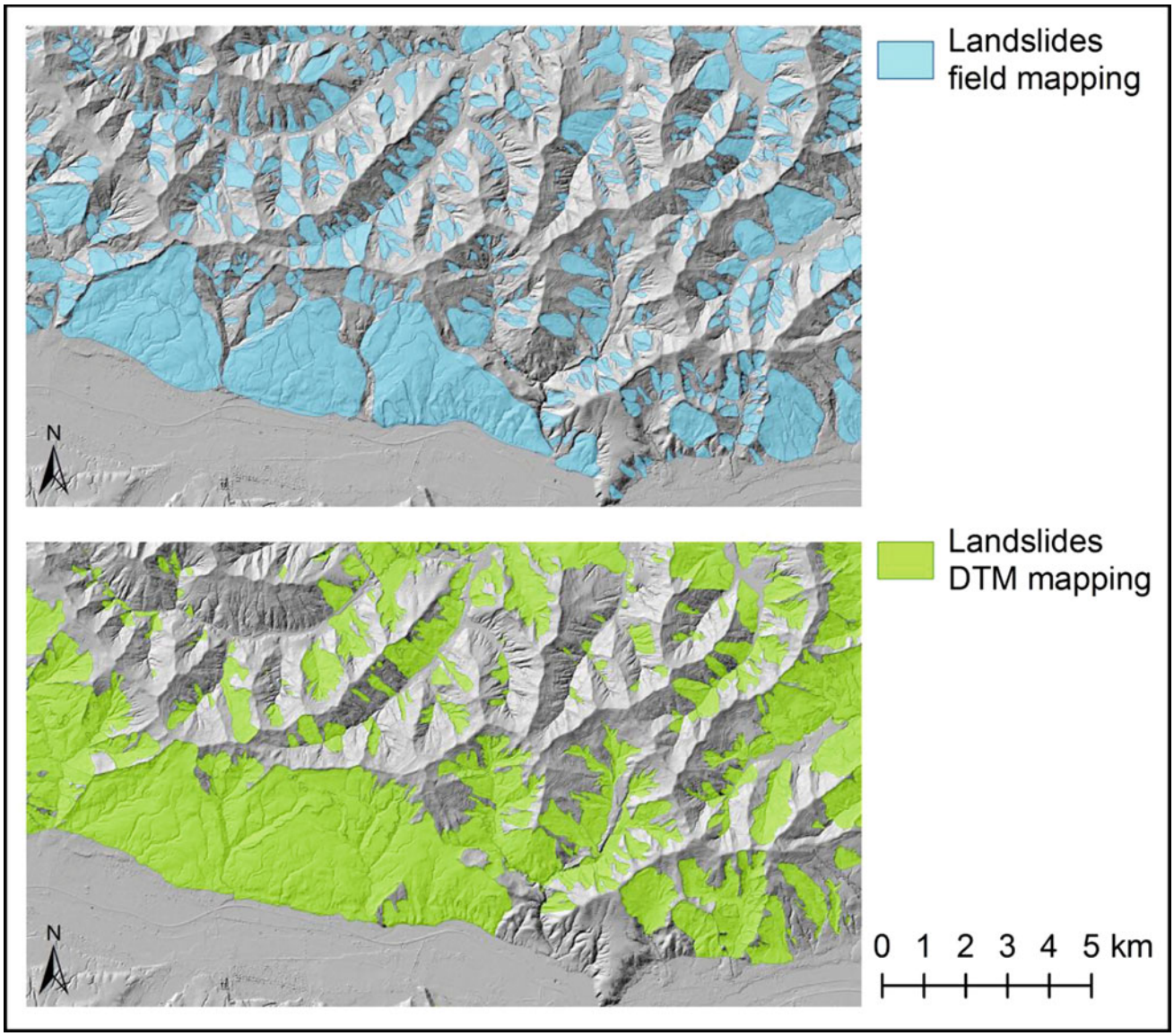

Fig. 5 Comparison of mapping results from field survey (*above*) and from DTM based mapping (*below*)

Discussion of the Methods and Conclusions

Comparing the 2 methodologies, advantages and disadvantages of each methodology should be discussed. DTM mapping was performed in only one week working time (1 person). This is a quarter of the time that was necessary to map the same area in the field. The DTM mapping was also solely accomplished from desk, making the mapping independent from weather conditions and other environmental influences and restrictions. On the other side, performing field survey enables the mapping team to identify the landslide geometric and morphological features directly. However, steep terrain and sometimes vegetation cover are restricting the field survey. The huge size of a lot of landslides combined with the strong anthropogenic transformation of the landscape (terraced agriculture) makes it also difficult to observe moving mechanisms and age of the landslides during fieldwork. As a result, some necessary information might be missed.

We believe that in our case, DTM mapping produced a more precise landslide inventory map than field work did. However, we also believe, that combining the two methodologies from the beginning on will be the best choice to create a state of the art landslide inventory map. A comparable experience was also described by Ardizzone et al. (2002). We have learned the lesson, that an ideal process should start with an overview mapping in the field, then DTM mapping should be performed and the results should then be crosschecked by field investigations. All team members that are involved in mapping (DTM or field based

work) should attend the overview mapping, whereas later tasks can also be performed by independent teams.

A most complete landslide inventory of the investigation area is not only an essential input factor for a landslide susceptibility model. It can also serve as an indicator map for itself, based on the fact, that existing moved masses are much more likely to become reactivated compared to unmoved masses (Leopold et al. 2013; Samia et al. 2016; Van Den Eeckhaut et al. 2009). Furthermore, in continuing work a proper landslide inventory can serve as statistical background for further investigations, as already described by Malamud et al. (2004).

One of the main results of the entire project was to demonstrate the applicability and the effectiveness of DTM mapping in Loess sediments of Western China. In comparison to field mapping, the DTM inventory is at least of equal quality as the field mapped inventory because of its consistency and completeness. Furthermore, DTM-mapping is much more cost efficient, especially with the outlook of mapping larger areas in Western China.

References

Ardizzone F, Cardinali M, Carrara A, Guzzetti F, Reichenbach P (2002) Impact of mapping errors on the reliability of landslide hazard maps. Nat Hazards Earth Syst Sci 2:3–14

Chen Y, Shi Y (2006) Basic characteristics of seismic landslides in loess area of Northwest China. J Seismol Res 29(3):276–281 (in Chinese)

Cheng Y, Zhang J, Du D (2007) On the relationship between fault activity and geological hazard in Tianshui Area, Gansu Province. J Eng Geol 15(01):33–37 (in Chinese)

Dou J, Chang K-T, Chen S, Yunus AP, Liu J-K, Xia H, Zhu Z (2015) Automatic case-based reasoning approach for landslide detection: integration of object-oriented image analysis and a genetic algorithm. Remote Sens 7(4):4318–4342

Gu G (1983) Catalogue of Chinese earthquakes: 1831 BC–1969 AD. Science Press, Beijing (in Chinese)

Gutjahr KH, Perko R, Raggam H, Schardt M (2014) The epipolarity constraint in stereo-radargrammetric DEM generation. IEEE Trans Geosci Remote Sens 52(8):5014–5022

Hirschmüller H (2008) Stereo processing by semi-global matching and Mutual Information. IEEE Trans Pattern Anal Mach Intell 30 (2):328–341

Kalbermatten M, Van De Ville D, Turberg P, Tuia D, St Joost (2012) Multiscale analysis of geomorphological and geological features in high resolution digital elevation models using the wavelet transform. Geomorphology 138(1):352–363

Kang L, Zhang X, Shi Y, Huang X, Li L (1999) A study on the earthquake risk segments of the North Fault Zone in West Qinling Mountain. South China J Seismol 19(1):60–65 (in Chinese)

Leopold Ph, Draganits E, Heiss G, Kovacs E (2013) A geotechnical explanation for the transition from creep to slides in the alpine foreland. In: Margottini C, Canuti P, Sassa K (eds) Landslide science and practice, vol 4. Global Environmental Change

Lu Y, Shi Y, Chen Y, Liu H (2006) Slippage estimation of the loess landslide triggered by eathquake. Northwestern Seismol J 28 (3):248–251 (in Chinese)

Malamud B, Turcotte D, Guzzetti F, Reichenbach P (2004) Landslide inventories and their statistical properties. Earth Surf Proc Land 29 (6):687–711

Pei X, Ding S, Li Y, Su C, Li Y, Chen S (2004) Tian shui shi fu (I48C 002003) 1: 250000 regional geological survey (revision surveys) achievements reports. Institute of geological survey, Chang'an University, Geology investigation institute in Gansu province, Xi'an, p 637 (in Chinese)

Perko R, Raggam H, Gutjahr KH, Schardt M (2014) Assessment of the mapping potential of Pléiades stereo and triplet data. In ISPRS annals of photogrammetry, remote sensing and SPATIAL information sciences, vol II-3, pp 103–109

Rumpler M, Wendel A, Bischof H (2013) Probabilistic range image integration for DSM and true-orthophoto generation. Scandinavian conference on image analysis, pp 533–544

Samia J, Temme A, Bregt A, Wallinga J, Guzzetti F, Ardizzone F, Rossi M (2016) Do landslides follow landslides? Insights in path dependency from a multi-temporal landslide inventory. Landslides, doi:10.1007/s10346-016-0739-x

Scharstein D, Szeliski R (2002) A taxonomy and evaluation of dense two frame stereo correspondence algorithms. Int J Comput Vision 47(1–3):7–42

Shao Y, Yuan D, Wang A, Liang M, Liu K, Feng J (2011) The segmentation of rupture and estimate of earthquake risk along the north margin of western Qinling fault zone. Seismol Geol 33(1):79–90 (in Chinese)

Van Den Eeckhaut M, Muys B, Van Loy K, Poesen J, Beeckman H (2009) Evidence for repeated re-activation of old landslides under forest. Earth Surf Proc Land 34(3):352–365

Wang M, Hu F, Li J (2011) Epipolar resampling of linear pushbroom satellite imagery by a new epipolarity model. ISPRS J Photogram Remote Sens 66(3):347–355

Wang N, Wang L (2013) Characteristics and influencing factors of seismic loess slopes in valley areas. Chin J Geotech Eng 35 (supp. 1):434–438 (in Chinese)

Zhang S, Xie Y (1991) The shallow geological tectonic in Tianshui earthquake area. Northwestern Seismol J 13(Supp.):22–28 (in Chinese)

Zhou M, Li Q, Min X, Fan B, Wei D (1991) The interpretation of the fanprofiles data in Tianshui earthquake area. Northwestern Seismol J 13(Supp.):44–47 (in Chinese)